ACS Catalysis

Research Article

pubs.acs.org/acscatalysis

Low-Valent Iron Mono-Diazadiene Compounds: Electronic Structure and Catalytic Application

Crispin Lichtenberg,*[,†] Mario Adelhardt,[‡] Thomas L. Gianetti,[†] Karsten Meyer,[‡] Bas de Bruin,[§] and Hansjörg Grützmacher*[,†]

[†]Department of Chemistry and Applied Biosciences, ETH Zürich, CH-8093 Zürich, Switzerland

[‡]Department of Chemistry & Pharmacy, Friedrich-Alexander University, Erlangen-Nürnberg (FAU), Egerlandstraße 1, D-91058 Erlangen, Germany

[§]van 't Hoff Institute for Molecular Sciences, Department of Homogeneous Catalysis, Faculty of Science, Universiteit van Amsterdam, Postbus 94720, 1090 GS Amsterdam, The Netherlands

Supporting Information

ABSTRACT: A series of monodiazadiene diolefin iron compounds, [Fe(trop$_2$dad)(L)] (**4**; L = neutral ligand), has been prepared by one-electron oxidation of the Fe^I species [NaFe(trop$_2$dad)(thf)$_3$] (dad = diazadiene; trop = 5*H*-dibenzo[*a*,*d*]-cyclohepten-5-yl). The electronic structures of compounds **4** were investigated by NMR and Mössbauer spectroscopy, single-crystal X-ray diffraction, solid- and liquid-phase magnetic susceptibility measurements, and DFT calculations. Compounds of type **4** with labile ligands L were found to be active (pre)catalysts for the dehydrogenative coupling of (alkyl)amine−boranes. Remarkably high activities were observed, especially for the homogeneous dehydrogenative polymerization of methylamine−borane.

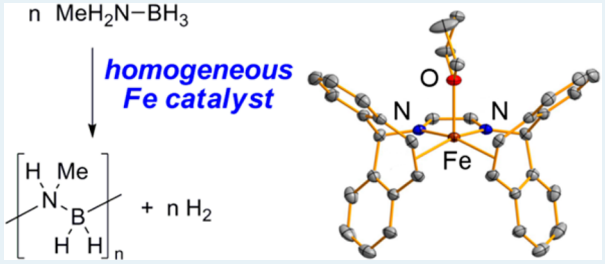

KEYWORDS: *iron diazadiene compounds, electronic structure determination, methylamine−borane, dehydrogenative polymerization, homogeneous catalysis*

INTRODUCTION

For decades, redox-active ligands have been investigated intensively from the coordination chemists' point of view.[1] More recently they have also been recognized as functional entities in homogeneously catalyzed reactions.[2] Specifically, it was suggested that direct participation of such a ligand in redox events within a catalytic cycle is advantageous in the case of first-row transition-metal catalysts.[3] The in-depth characterization of compounds containing redox-active ligands remains challenging, however, since electronic coupling between metal- or ligand-centered unpaired local spins can obscure the true electronic structure of the overall compound.

Diazadienes (dads) represent a prominent class of redox-active ligands. Examples of iron compounds with one or two diazadiene ligands, [Fe(dad)(L$^\pi$)$_n$] (L$^\pi$ = π-acidic ligand) and [Fe(dad)$_2$], were reported early on.[4,5] However, it was only recently that the correct electronic structure of bis(diazadiene) compounds [Fe(dad)$_2$] was revealed by a combination of spectroscopic, crystallographic, and theoretical techniques and methods.[6,7] These compounds are best described as high-spin Fe^{II} centers (local spin S_{Fe} = 2) antiferromagnetically coupled to two monoanionic dad radical ligands, (dad)$^{\bullet-}$ (local spin S_{dad} = 1/2), which results in an overall S = 1 ground state. In contrast, the electronic structure of monodiazadiene species [Fe(dad)(L$^\pi$)$_n$] has remained largely unexplored.

Some catalytic applications of [Fe(dad)(L$^\pi$)$_n$], [Fe(dad)(X)$_2$] (X = halide), and [Fe(dad)$_2$] have been reported. They include the hydrogenation of 1-hexene,[8] (cyclo)dimerizations of dienes,[5,9] cyclotrimerizations of alkynes,[10] Diels−Alder type cyclizations of dienes with alkynes,[10] and olefin polymerizations[11] and require the addition of an external activator or initiator. Iron diazadiene compounds as catalysts for dehydrogenation reactions have not yet been reported to our knowledge. We described the anionic Ru hydride complex [RuH(trop$_2$dad)] with a tetradentate diolefin diazadiene ligand (trop = 5*H*-dibenzo[*a*,*d*]cyclohepten-5-yl) as a highly active catalyst for the dehydrogenation of methanol/water mixtures or pure formic acid to CO_2 and H_2.[12] We became interested in the development of a related iron-based homogeneous catalyst for dehydrogenative oligo- and polymerization reactions that does not require an additional activator. In recent work, we showed that a multidentate trop-based diolefin diamido ligand, (trop$_2$dae)$^{2-}$ (see **5** in Scheme 1), which is the hydrogenated version of the unsaturated trop$_2$dad ligand, stabilizes low-valent iron centers.[13a] One of the main challenges under the inherently reducing reaction conditions is

Received: July 7, 2015
Revised: September 12, 2015
Published: September 15, 2015

DOI: 10.1021/acscatal.5b01416
ACS Catal. 2015, 5, 6230−6240

Scheme 1. Synthesis of [Fe(trop$_2$dad)(L)] (4a–d) (Including Unsuccessful Approaches) and Chemically Reversible Interconversion of 2 and 4a

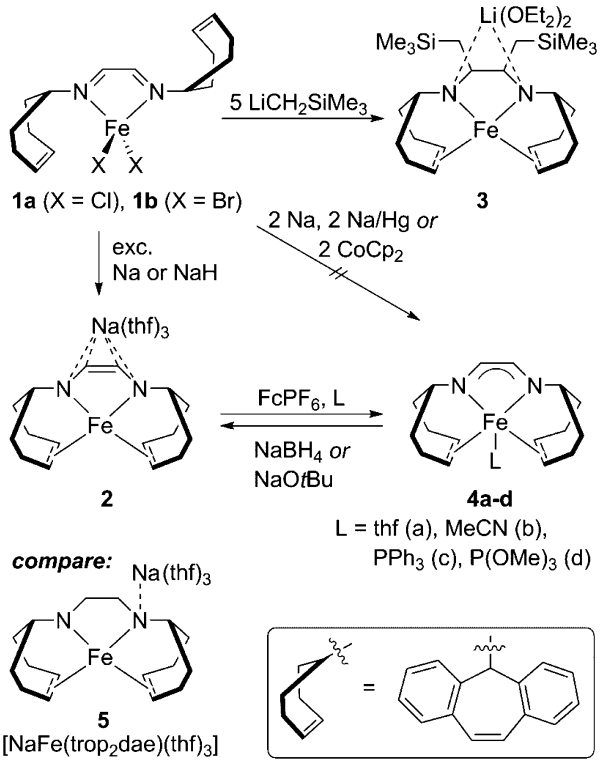

to prevent catalyst deactivation or modification by formation of small Fe particles.[13−15]

Here we report the synthesis, electronic structure investigation, and reactivity of the iron diolefin diazadiene compounds [Fe(trop$_2$dad)(L)] (L = neutral ligand). These compounds are among the most active base-metal catalysts for the dehydrogenative polymerization of methylamine−borane.

RESULTS AND DISCUSSION

Synthesis of Low-Valent Fe Compounds. The low-valent iron diazadiene ate compound [NaFe(trop$_2$dad)(thf)$_3$] (**2**) can be accessed from [FeBr$_2$(trop$_2$dad)] (**1b**) with an excess of elemental sodium or NaH as reducing agent (Scheme 1).[16] The anionic part of this contact ion pair contains a low-spin (ls) d^7-Fe^{I} center to which a diamido ethylene ligand is coordinated: that is, the two-electron -reduced form (trop$_2$dad)$^{2-}$. Electrochemical data suggest that the product of a one-electron oxidation of **2**, that is, the neutral complex [Fe(trop$_2$dad)], should be a stable compound. However, attempts to prepare such a complex in a stoichiometric reaction from **1a** or **1b** failed. Lithium or sodium alkyls such as [MCH$_2$SiMe$_3$] (M = Li, Na) have been successfully used as homogeneous reducing agents for Fe^{II} halides with diazadiene or the saturated diaminoethylene ligand (H$_2$trop$_2$dae), which gives **5** as a product.[6a,13a,17] However, the reaction of [FeCl$_2$(trop$_2$dad)] (**1a**) with [LiCH$_2$SiMe$_3$] resulted in a nucleophilic attack on the two imine functionalities and concomitant single-electron reduction of the iron center to give the ls Fe^{I} species **3**, which was isolated and characterized (for further details see the Supporting Information). Stoichiometric reactions of **1b** with 2 equiv of Na, Na/Hg, or [CoCp$_2$] as the reducing agent gave low yields of compound **2**, free ligand, or [Fe^{II}(trop$_2$dad)$_2$],[16] respectively, as the only isolable products. Thus, we pursued oxidation of **2**, rather than reduction of **1a,b**, as a synthesis strategy. Indeed, the reaction of **2** with 1 equiv of ferrocenium hexafluorophosphate gave intensely dark red [Fe(trop$_2$dad)(thf)] (**4a**) in 81% yield, which was isolated with 0.5 equiv of [Na(thf)$_5$PF$_6$] per formula unit in the crystal lattice. With similar protocols, dark brown compounds [Fe(trop$_2$dad)(L)] (**4b–d**) could be isolated, where the thf ligand bound to the Fe center has been replaced by another σ donor (L = MeCN (**4b**)) or by a σ donor/π acceptor ligand (L = PPh$_3$ (**4c**), P(OMe)$_3$ (**4d**)). The chemical reversibility between ion pair **2** and neutral species of type **4** was demonstrated by the reaction of **4a** with mild reducing agents such as NaBH$_4$ and NaO*t*Bu, from which compound **2** was isolated in 60−66% yield.

Compounds **4a–d** were characterized by single-crystal X-ray diffraction studies (Figure 1, Table 1, and the Supporting Information). The Fe centers are five-coordinate, residing in square-pyramidal (τ_5 = 0 (**4a**)), 0.10 (**4b**)), intermediate (τ_5 = 0.50 (**4d**)), and distorted-trigonal-bipyramidal coordination geometries (τ_5 = 0.60 (**4c**)).[18] The monodentate ligand occupies the apical position in **4a,b**, whereas it is found in an equatorial position in **4c**. The changes in the coordination geometry from **4a,b** to **4c,d** are attributed to steric (**4c,d**) and electronic effects (**4c**: $\pi-\pi$ interactions between the phenyl and benzo groups). The average Fe−N and Fe−(C=C^{trop}) bond lengths (1.89−1.92 and 1.97−2.00 Å) are within the range of those previously described for five-coordinate monodiazadiene iron compounds (1.89−1.93 and 1.97 Å) (C=C^{trop} = olefinic binding sites).[8,19] Note that the C=C^{trop} and N units in axial positions in **4c,d** interact more weakly with the Fe center than their counterparts in equatorial positions. This is ascribed to a thermodynamic trans effect and is reflected in longer Fe−(C=C^{trop})/Fe−N and shorter C=C^{trop} distances (Supporting Information). The C−C^{dad} and C−N^{dad} bond lengths in the diazadiene ligand backbone are an important measure of the oxidation state of this type of ligand.[6,20] In compounds **4a–d**, these distances are intermediate between those in

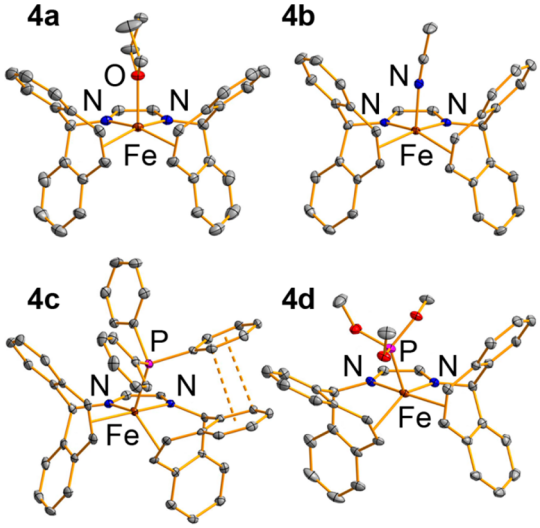

Figure 1. Molecular structures of **4a–d**. Displacement ellipsoids are shown at the 50% probability level. H atoms, cocrystallized [Na(thf)$_5$PF$_6$] in the case of **4a**, and solvent molecules in the lattice are omitted for clarity.

DOI: 10.1021/acscatal.5b01416
ACS Catal. 2015, 5, 6230−6240

Table 1. Selected Bond Lengths (Å) and τ_5 Values for Compounds 4a−d

	4a (L = thf)	4b (L = NCMe)	4c (L = PPh_3)	4d (L = $P(OMe)_3$)
τ_5	0	0.10	0.60	0.50
$C{=}C^{olefin}$	1.423(3)	1.420(4)[a]	1.434(5)[a,b]	1.430(2)[a,b]
Fe−N	1.9203(17)	1.907(2)[a]	1.910(3)[a,b]	1.8928(13)[a,b]
Fe−(C=C)	1.974(2)	1.991(3)[a]	2.000(4)[a,b]	1.9855(15)[a,b]
Fe−E	2.141(2)	1.999(2)	2.3202(11)	2.1939(4)
$C{-}C^{backbone}$	1.402(4)	1.389(4)	1.389(5)	1.392(2)
C−N	1.325(3)	1.331(3)[a]	1.326(5)[a]	1.3315(19)[a]

[a]Mean value. [b]Individual values differ considerably (see text).

$[FeX_2trop_2dad]$ (**1a,b**) with a neutral $trop_2dad$ ligand (two short $C{=}N^{dad}$ bonds and one long $C{-}C^{dad}$ bond) and those in $[NaFe(trop_2dad)(thf)_3]$ (**2**) with a fully reduced dianionic $(trop_2dad)^{2-}$ ligand (two long $C{-}N^{dad}$ bonds and one short $C{=}C^{dad}$ bond). In **4a−d** the $C{-}N^{dad}$ and $C{-}C^{dad}$ bond lengths are similar to those reported for $[Fe^{II}(trop_2dad)_2]$ and other Fe diazadiene compounds, which all contain monoanionic radical $(dad)^{\bullet-}$ ligands.[6,16] These structural data suggest monoanionic radical $(trop_2dad)^{\bullet-}$ ligands for compounds **4a−d** and consequently an Fe^{I} oxidation state. Other five-coordinate iron dad compounds with π-acidic ligands show comparable bonding parameters for the ligand backbone, although minor deviations occur in some cases.[6,9b,19]

It has been stated that the changes of the bonding parameters with respect to the free ligand are due to π back-donation, and molecular orbital calculations have been performed for a model compound.[19b,c] However, the recent detailed insights into the electronic structures of $[Fe(dad)_2]$-type compounds called for a deeper investigation of the electronic structures of **4a−d**.

Electronic Structure of Low-Valent Fe Compounds. Zero-field ^{57}Fe Mössbauer spectroscopy of solid **4a−d** at 77 K revealed a clean quadrupole doublet in each case, ruling out the presence of Fe-based impurities (Table 2 and the Supporting Information). **4a−d** show isomer shifts of 0.43−0.22 mm/s, which are close to the isomer shifts observed for ls Fe^{I} centers coordinated by the bis(trop)diazadiene ligand as in $[Fe_3(trop_2dad)_2]$ (δ = 0.37(1) mm/s) and ($[NaFe(trop_2dad)(thf)_3]$ (**2**; δ = 0.21(1) mm/s). This result clearly excludes a hs Fe^{II} electron configuration.[16,21] The lower isomer shifts for **4c,d** with their π-acidic phosphorus ligands in comparison to **4a,b** indicate a higher s electron density at Fe, which is a result of effective d(Fe) → σ^*(P−R) electron back-donation. In the case of **4c,d**, where a direct comparison of all Fe−ligand bond lengths is possible, shorter Fe−ligand bonds expectedly lead to a smaller isomer shift (Tables 1 and 2).[21] The quadrupole splittings of **4a−d** range from 1.11 to 1.69 mm/s.

Table 2. Zero-Field ^{57}Fe Mössbauer Parameters for 4a−d

	4a (L = thf)	4b (L = NCMe)	4c (L = PPh_3)	4d (L = $P(OMe)_3$)
δ (mm/s)	0.43(1)	0.42(1)	0.33(1)	0.22(1)
ΔE_Q (mm/s)	1.69(1)	1.11(1)	1.31(1)	1.16(1)

SQUID magnetic susceptibility measurements were performed for **4a** as a representative example (solid state, 1 T) and indicate that this compound is diamagnetic over a temperature range of 2−300 K. Frozen solutions of **4a** in THF at 91 K are EPR silent. The experimental results therefore suggest that compounds **4a−d** are best described as ls Fe^{I} centers with strong antiferromagnetic coupling to their monoanionic radical $(trop_2dad)^{\bullet-}$ ligands, although a closed-shell singlet electronic structure, ls $Fe^0\{L^0\}$ ↔ ls $Fe^{II}\{L^{2-}\}$ (π back-donation model), with a net Fe^{I} oxidation state, cannot be fully excluded (vide infra). Thus, upon one-electron oxidation of $[NaFe(trop_2dad)(thf)_3]$ (**2**), one electron is removed from the redox-active ligand rather than from the metal center to give compounds of type **4**. This is in contrast with previous findings on the related iron bis(diiminobenzosemiquinonate), where a one-electron oxidation takes place at the metal center.[22]

In order to gain further support for the electronic structure assignment, we performed DFT calculations on the full atom models of $[Fe(trop_2dad)(thf)]$ (**4a**) and $[Fe(trop_2dad)]$ (**4e**).[23] Geometries were optimized with Turbomole at the DFT-D3, hybrid b3-lyp, def2-TZVP level, employing Grimme's version 3 dispersion corrections, in three different electronic configurations: closed-shell singlet (S = 0; spin-restricted singlet), open-shell singlet (S = 0; spin-unrestricted singlet, broken symmetry approach), and triplet (S = 2; spin unrestricted) (Table 3).

Table 3. DFT Computed ZPE Corrected SCF Energies (kcal mol^{-1}) of Species 4a,e in Different Electronic Configurations

	closed-shell singlet (S = 0)	triplet (S = 1)	open-shell singlet[a] (S = 0)
4a	0	−9.2 ($\langle S^2\rangle$ = 2.0341)	−16.2 ($\langle S^2\rangle$ = 1.0799)
4e	0	−19.0 ($\langle S^2\rangle$ = 2.0216)	−22.0 ($\langle S^2\rangle$ = 1.1594)

[a]Energy corrected for triplet spin contamination.

The closed-shell singlet configuration is perhaps best described with two resonance structures that contribute equally to the electronic ground state, ls $Fe^0\{L^0\}$ ↔ ls $Fe^{II}\{L^{2-}\}$, one of which contains a neutral, low-spin d^8 iron(0) center supported by a neutral $trop_2dad$ ligand ($Fe^0\{L^0\}$) and the other contains a dicationic, low-spin d^6 iron(+II) center supported by a dianionic $trop_2dad^{2-}$ ligand ($Fe^{II}\{L^{2-}\}$). This description reflects a ligand to metal σ,π donation and metal to ligand π back-donation model. This model effectively corresponds to a net Fe^{I} system, but without invoking radical density on either the metal or the ligand. In contrast, the triplet and the open-shell singlet configurations are both best described as metallo-radical ligand radical $Fe^{I}\{L^{\bullet-}\}$ species, each containing a monocationic, low-spin d^7 iron(+I) center (S = 1/2) supported by a monoanionic $trop_2dad^{\bullet-}$ radical-type ligand (S = 1/2). They differ in the exchange-coupling interaction between the unpaired electrons centered on the metal and the ligand. In the open-shell singlet configuration these are *antiferro*magnetically coupled (leading to an overall S = 0 ground state), while in the triplet configuration they are *ferro*magnetically coupled (leading to an overall S = 1 ground state), as reflected by the spin density plots shown in Figure 2.

DOI: 10.1021/acscatal.5b01416
ACS Catal. 2015, 5, 6230−6240

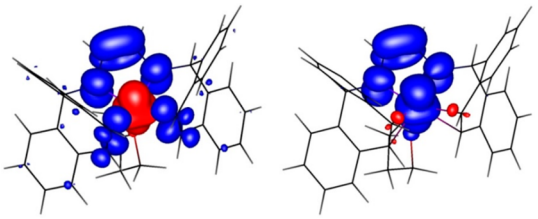

Figure 2. Spin density plots of open-shell singlet (left) and triplet (right) configurations of **4a**.

For both **4a** and **4e**, the triplet and open-shell singlet configurations are computed to be significantly stabilized over the respective closed-shell singlet configuration (Table 3), suggesting that these complexes might indeed be best described as $Fe^{I}\{L^{\bullet-}\}$ species. For the thf adduct **4a**, the open-shell singlet configuration is significantly stabilized over the triplet configuration, which is in agreement with the diamagnetic ground state of this species as determined experimentally. For complex **4e** without thf, the computed triplet and open-shell singlet energies are much closer, which is in congruency with the experimentally observed paramagnetic shift and line broadening of the NMR signals of these complexes in solution (vide infra). As such, the data are consistent and are suggestive of electronic structures best described as (antiferromagnetically coupled) $Fe^{I}\{L^{\bullet-}\}$ "ligand radical" complexes (for a more detailed discussion, see the Supporting Information). However, predicting relative energies of species in different spin state configurations with DFT methods can be troublesome, and the same can be expected when comparing the relative energies of closed-shell and open-shell singlet configurations.[24] The assignment of neutral Fe(bpy)-type complexes containing redox-active bipyridine (and related) ligand scaffolds as an antiferromagnetically coupled $Fe^{I}\{L^{\bullet-}\}$ species on the basis of DFT studies has recently been challenged on the basis of high-level CASSCF ab initio computations.[25] High-level multi-reference ab initio methods (such as CASSCF) can accurately describe the electronic structure of open-shell singlet species but are (currently) too expensive for geometry optimizations (certainly for large systems such as complex **4a**). Combined with the fact that the geometries and energies of **4a** in the three different electronic structures under consideration are mutually dependent and vary widely (at least, according to DFT), comparing high-level ab initio single-point energies of different spin configurations, without performing geometry optimizations at the same level, could easily produce erroneous results due to a mismatch between the electronic structure and its optimal geometry. As such, it is doubtful if any of the currently available computational methods are able to unequivocally distinguish between open-shell singlet $Fe^{I}\{L^{\bullet-}\}$ and closed-shell singlet $Fe^{0}\{L^{0}\} \leftrightarrow Fe^{II}\{L^{2-}\}$ descriptions of species such as **4a**. Both descriptions correspond to a (net) Fe^{I} system, and hence both descriptions in principle are in agreement with the experimental data. Furthermore, to the best of our knowledge, there are also no experimental methods available to unequivocally discriminate between closed-shell and open-shell singlet species in a straightforward manner, if the exchange coupling in the latter is strongly antiferromagnetic (thus leading to completely diamagnetic systems in both cases). Its low DFT energy in comparison to the closed-shell solution of **4a** is perhaps in favor of an open-shell singlet $Fe^{I}\{L^{\bullet-}\}$ ligand radical description. However, considering developments in the field[25] and the well-known problems associated with assigning spin states on the basis of (hybrid) DFT calculations, we refrain from drawing any firm conclusions on this matter.

Compound **4a** is not diamagnetic in solution.[26] It shows a low effective magnetic moment in solution, which can be ascribed to an equilibrium according to [Fe(trop$_2$dad)(thf)] (**4a**) ⇆ [Fe(trop$_2$dad)] (**4e**) + THF.[27] In agreement with this equilibrium, the observed effective magnetic moment is much smaller than that expected for pure $\mathbf{4e}^{\mathbf{triplet}}$ ($\mu_{expected}$ = 2.83 μ_B for g = 2.0); it is solvent dependent (μ_{eff}(C_6D_6, 298 K, 0.02 M) = 1.9(1) μ_B, μ_{eff}(THF-d_8, 298 K, 0.02 M) = 1.3(1) μ_B), concentration dependent (μ_{eff}(C_6D_6, 298 K, 0.02 M) = 1.9(1) μ_B, μ_{eff}(C_6D_6, 298 K, 0.01 M) = 2.2(1) μ_B), and temperature dependent (μ_{eff}(Tol-d_8, 298 K, 0.02 M) = 1.8(1) μ_B, μ_{eff}(Tol-d_8, 243 K, 0.02 M) = 1.3(1) μ_B).[28] An isotropic shift analysis of a 0.02 M toluene solution of **4a** in the temperature range 233–298 K supports an equilibrium between singlet and triplet species (for details see the Supporting Information). Likewise, compounds **4b,c** show low magnetic moments in solution,[29] whereas **4d** is diamagnetic and, as expected, is EPR silent (see the Experimental Section). Similar to the phenomenon described above, iron porphyrins show different spin states depending on the presence/absence and nature of additional neutral ligands.[30] The possibility of controlling the spin state of a metal complex by the choice of a neutral ligand has been described for a trinuclear all-ferrous compound.[31,32]

In THF-d_8 solution, NMR spectroscopic analysis of **4a** reveals apparent C_{2v} symmetry, even at temperatures as low as −40 °C. Thus, **4a** undergoes a rapid transformation, by which its thf ligand is transferred from one side of the Fe–diazadiene plane to the other. For compound **4b**, an analogous process takes place at 25 °C in MeCN-d_3 solution (apparent C_{2v} symmetry). However, it is slow on the NMR time scale at −30 °C, as apparent C_2 symmetry is observed at this temperature. The neutral ligands in compounds **4a,b** are labile in THF/MeCN solution, as shown by ^{1}H NMR spectroscopy. Therefore, the dynamic processes described above are likely to be intermolecular: that is, associated with a dissociation and association step of L. Similarly, the PPh_3 ligand in **4c** is labile, as suggested by similar ^{1}H NMR spectra for **4b,c** in MeCN-d_3 solution and by a very broad resonance in the ^{31}P NMR spectrum of **4c** in the same solvent. In contrast, compound **4d** shows apparent C_2 symmetry in MeCN-d_3 already at 25 °C and no rapid displacement of the $P(OMe)_3$ ligand is observed. Overall, the ease of displacement of the neutral ligands in compounds **4a–d** by THF or MeCN follows the reverse trend of the ligands' π-acidities: THF > MeCN > PPh_3 > $P(OMe)_3$.

Catalyzed Dehydrogenations. Initiated by the pioneering work of Manners and Baker,[33] (alkyl)ammonia–boranes, $RH_2N{\cdot}BH_3$ (R = alkyl, H), have been discussed as hydrogen storage devices[34] and can be utilized as hydrogen transfer reagents.[34c,35] Moreover, they have been in the focus of research efforts as precursors for the synthesis of oligo- or polymeric BN materials.[33b,34c] Polymeric compounds obtained from catalyzed dehydrocouplings of (alkyl)ammonia–boranes are isoelectronic with polyolefins and graphene but show different material properties due to the more polar nature of the BN bond. Potential applications for such materials include high-performance polymers[34,36] and the use as a graphene support for (opto)electronic devices.[37] Whereas methods for the synthesis of hydrocarbon polymers have been highly elaborated, those for the synthesis of the BN analogues still have the potential for further developments. For methylammonia–borane, $MeH_2N{\cdot}BH_3$ (MAB), dehydrocoupling can result

DOI: 10.1021/acscatal.5b01416
ACS Catal. 2015, 5, 6230–6240

in the formation of the cyclic trimer $[MeHN\text{-}BH_2]_3$,[38] *N*-trimethylborazine ($[MeN\text{-}BH]_3$), or poly-MAB ($[MeHN\text{-}BH_2]_n$). The outcome of the reaction depends not only on the choice of catalyst but also on the reaction conditions. Whereas some precious-metal catalysts can be used to generate poly-MAB,[33b,36,39] only a very limited number of base-metal catalysts have been reported for this reaction:[40] $[Mn(C_5H_5)(CO)_3]$, $[Cr(C_6H_6)(CO)_3]$, and $[Fe(C_5H_5)\text{-}(CO)_2]_2$ catalyze the dehydrogenative polymerization of MAB in reaction times of 3−12 h but require constant UV irradiation.[41]

Compounds **4a**,**b** were tested as catalysts for the dehydrogenative polymerization of MAB with 5 mol % catalyst loading in toluene solution in an open system at 23 °C (Table 4, entries 1 and 2). In both cases, full conversion was observed after 8.5 min, as indicated by the release of 1 equiv of H_2, with virtually no small cyclic BN products being detected. Once isolated as a colorless solid, the poly-MAB product shows poor solubility in common organic solvents and was identified by IR spectroscopy. Mass spectrometry revealed signals of up to m/z 943, indicating at least 22 repeating units. This makes **4a**,**b** the most active base-metal catalysts for the dehydrogenative polymerization of MAB. A turnover frequency of 5.1×10^{-2} s^{-1} was determined for these reactions on the basis of the linear region of the time/conversion plot (ca. 2−6 min reaction time).[42] In order to determine if the dehydrogenative polymerization of MAB proceeds via a chain growth or a step growth mechanism, reactions were stopped before full conversion was reached. Analysis of the oligo-/polymeric material showed molecular weights clearly exceeding those predicted for a step growth mechanism using Carothers' equation and thus suggests a chain growth mechanism to be operative, as reported for an iridium-catalyzed MAB dehydrogenation.[39b] Lowering the catalyst loading to 1 mol % resulted in 95% conversion after 20 min (entry 3). When 3 × 20 equiv of MAB was used as a substrate in consecutive additions, full conversion was observed in each cycle, with much greater reaction times being necessary for the second and third cycles (entry 4). This suggests partial catalyst degradation, although no color change was observed during the reaction.[43,44]

Table 4. Catalyzed Dehydrogenative Polymerization of Methylamine−Borane (MAB)[a]

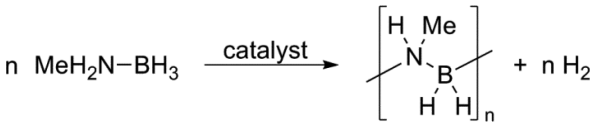

entry	cat.	additive (amt (equiv))	t (min)	conversion (%)
1	**4a**		8.5	>99
2	**4b**		8.5	>99
3	**4a**[b]		20	95
4	**4a**		8.5/99/186	3 × >99
5	**4a**	THF as solvent	101	>99
6	**4a**	$P(OMe)_3$ (0.1)[c]	11	>99
7	**4a**	$P(OMe)_3$ (0.2)[c]	12	>97
8	**4a**	$P(OMe)_3$ (2.0)[c]	15	63
9	**2**		227	70
10	**5**		15	<1

[a]Conditions unless specified otherwise: 5 mol % catalyst, toluene, 23 °C, open system. [b]1 mol % catalyst. [c]Added after 2.5 min reaction time.

Reactions with catalysts **4a**,**b** show a short induction period, indicating that these compounds are not the catalytically active species. Formation of the active species could be a process such as substitution of the neutral ligand THF/MeCN for a substrate molecule, or it could involve reduction of the molecular iron compounds to give catalytically active small Fe particles. For precious-metal catalysts, it has been demonstrated that both homogeneous and heterogeneous regimes are operative in MAB dehydrogenations.[38b,39c] To our knowledge, this question has not been addressed for MAB dehydrogenation using base-metal catalysts.[45] Increasing the polarity of the solvent (from toluene to THF) drastically lowers the rate of reaction, hinting at a homogeneous regime (entry 5). Selective poisoning experiments[46] with 0.1 or 0.2 equiv of $P(OMe)_3$ per Fe being added to a running reaction still give full conversion after slightly increased reaction times, whereas addition of 2.0 equiv of $P(OMe)_3$ per Fe shuts down the catalytic activity (entries 6−8 and the Supporting Information). These results indicate that in situ generated **4d** is not an active (pre)catalyst for MAB dehydrogenation and also disfavors a scenario with catalytically active Fe particles. In comparison to **4a**,**b**, the related, singly reduced species **2** is only moderately active in MAB dehydrogenation and an analogous Fe^I compound with a saturated ligand backbone, $[NaFe(trop_2dae)(thf)_3]$ (**5**),[13a] is not active (dae = $-CH_2-CH_2-$) (entries 9 and 10).

When the substrate was changed to either amine−borane, $H_3N{\cdot}BH_3$ (AB), or dimethylamine−borane, $Me_2HN{\cdot}BH_3$ (DMAB), 5 mol % of compound **4a** induced full to high conversion with respect to release of 1 equiv of H_2 (Table 5 entries 1 and 2).[47] Whereas the data still indicate high catalytic activity for these reactions among homogeneous Fe-based catalysts, heterogeneous Fe-based catalysts are more active[14,48] and the outstanding performance of **4a**,**b** in MAB dehydrogenation was not reached. These results demonstrate how subtle changes in the electronic and steric profile of the (alkyl)amine−borane substrate can have drastic effects on a homogeneous catalyst's performance. The trend in the precatalysts' activity for MAB dehydrogenation, **4a** > **2** > **5**, is maintained for AB

Table 5. Catalyzed Dehydrogenative Polymerization of Amine−Borane (AB) and Cyclodimerization of Dimethylamine−Borane (DMAB)[a]

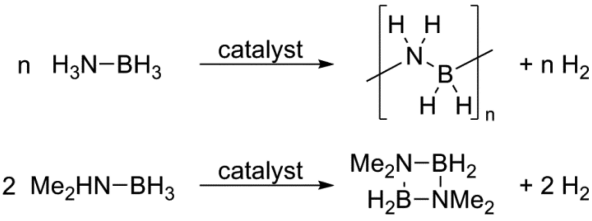

entry	cat.	monomer	solvent	t (min)	conversion (%)
1	**4a**	AB	THF[b]	300	>99
2	**4a**	DMAB	Tol	385	80
3	**2**	AB	THF[c]	210	12
4	**2**	DMAB	Tol	240	95
5	**5**	AB	MTBE	26	<1
6[13a]	**5**	DMAB	Tol	240	>99

[a]Conditions: 5 mol % catalyst loading, 23 °C, open system. [b]Similar results with toluene as a solvent (298 min, 93%). [c]With toluene as a solvent, a higher rate of reaction is observed (106 min, 77%), but full conversion is not reached and poisoning experiments with 0.1 equiv of $P(OMe)_3$ per Fe suggest heterogeneous conditions.

DOI: 10.1021/acscatal.5b01416
ACS Catal. 2015, 5, 6230−6240

(entries 3 and 5), but similar activities are apparent for DMAB (entries 4 and 6).

CONCLUSIONS

The Fe^{I} compound [NaFe(trop$_2$dad) (thf)$_3$] (**2**) with a redox-active diazadiene (dad) diolefin ligand is susceptible to a chemically reversible one-electron oxidation to give the series of compounds [Fe(trop$_2$dad)(L)] (**4**; L = thf (**4a**), MeCN (**4b**), PPh_3 (**4c**), $P(OMe)_3$ (**4d**); trop = 5*H*-dibenzo[*a*,*d*]-cyclohepten-5-yl). Compounds **4** were studied by techniques including single-crystal X-ray analysis, magnetic susceptibility measurements, Mössbauer spectroscopy, and DFT calculations. On the basis of these investigations, we tentatively assign an open-shell singlet electronic structure to compounds **4** with a ls Fe^{I} center antiferromagnetically coupled to a monoanionic ligand radical (trop$_2$dad)$^{\bullet-}$ (S_{total} = 0), although a closed-shell singlet electronic structure, ls $Fe^{0}\{L^{0}\}$ ↔ ls $Fe^{II}\{L^{2-}\}$, with a net Fe^{I} oxidation state remains possible. Solution magnetic susceptibility measurements and DFT calculations on **4a** suggest that the paramagnetic species [Fe(trop$_2$dad)] (**4e**) with a dissociated thf ligand is formed in an equilibrium reaction. In compounds **4**, the s electron density at Fe responds to the π acidity of the neutral ligand following the order thf ≈ MeCN < PPh_3 < $P(OMe)_3$, as evidenced by Mössbauer spectroscopy. Compounds **4a**,**b** were investigated as (pre)-catalysts for the dehydrogenative coupling of (alkyl)amine−boranes. They are the most active (pre)catalysts containing a relatively cheap and abundant metal for the dehydrogenative polymerization of methylamine−borane (MAB). Selective poisoning experiments suggest a homogeneously catalyzed reaction. This gives further evidence for the efficiency of trop type ligands to stabilize low-valent iron centers under reducing conditions in catalysis, although Fe catalysts with even longer lifetimes under catalytic conditions would be desirable. With amine−borane and dimethylamine−borane as substrates, high catalyst activities were observed, although the outstanding performance with MAB is not reached. This exemplifies once more the sensitivity of the catalyst systems to minor steric and electronic changes of the substrate in dehydrocoupling reactions. In future work, the use of these and related low-valent iron complexes in other dehydrogenative coupling processes will be investigated.

EXPERIMENTAL SECTION

General Considerations. All air- and moisture-sensitive manipulations were carried out using standard vacuum-line Schlenk techniques or in an MBraun inert-atmosphere drybox containing an atmosphere of purified argon. C_6D_6, THF-d_8, and MTBE were distilled before use from sodium benzophenone ketyl. CD_2Cl_2 was distilled before use from CaH_2. THF, *n*-hexane, toluene, and MeCN were purified using an Innovative Technologies PureSolv system and stored over 4 or 3 Å molecular sieves, respectively. Sodium, mercury, NaO*t*Bu, [Co(C_5H_5)$_2$], $NaBH_4$, $Me_2HN{\cdot}BH_3$, $H_3N{\cdot}BH_3$, and anhydrous $FeBr_2$ were obtained from Sigma-Aldrich and used as received. NaH was obtained from Sigma-Aldrich as a dispersion in mineral oil and was washed with *n*-hexane and dried in vacuo prior to use. Trop$_2$dad, [$FeCl_2$(thf)$_{1.5}$], [Li(CH_2SiMe_3)], [NaFe(trop$_2$dae)(thf)$_3$], [Fe(C_5H_5)$_2$][PF_6], and $MeH_2N{\cdot}BH_3$ were synthesized according to the literature. NMR spectra were recorded on Bruker instruments operating at 200, 250, 300, 400, or 500 MHz with respect to ^{1}H. ^{1}H NMR chemical shifts are reported relative to $SiMe_4$ using the residual ^{1}H chemical shifts of the solvent as a secondary standard. ^{11}B NMR chemical shifts are reported relative to $BF_3{\cdot}OEt_2$. Infrared spectra were collected on a PerkinElmer Spectrum 2000 FT-IR-Raman spectrometer. UV/vis spectra were recorded on a UV/vis/NIR Lambda-19 spectrometer in a cell with a 0.5 cm path length. Elemental analyses were performed at the Mikrolabor of ETH Zürich. For mass spectrometric MALDI-TOF experiments, a Bruker UltraFlex II MALDI-TOF-MS instrument and a *trans*-2-[3-(4-*tert*-butylphenyl)-2-methyl-2-propenylidene]-malononitrile (DCTB) or 2,5-dihydroxybenzoic acid (DHB) matrix were used, and the laser power was adjusted to give appropriate peak intensities. Single crystals suitable for X-ray diffraction were coated with polyisobutylene oil in a drybox, transferred to a nylon loop, and then transferred to the goniometer of an Oxford XCalibur, Bruker ApexI, ApexII, or Venture diffractometer equipped with a molybdenum X-ray tube (λ = 0.71073 Å). The structures were solved using direct methods (SHELXS) completed by Fourier synthesis and refined by full-matrix least-squares procedures. CCDC 1409557−1409562 contain crystallographic information for compounds **1a**, **3**, and **4a**−**d**. ^{57}Fe Mössbauer spectra were recorded on a WissEl Mössbauer spectrometer (MRG-500) at 77 K in constant-acceleration mode. ^{57}Co/Rh was used as the radiation source. WinNormos for Igor Pro software has been used for the quantitative evaluation of the spectral parameters (least-squares fitting to Lorentzian peaks). The minimum experimental line widths were 0.20 mm/s. The temperature of the samples was controlled by an MBBC-HE0106 Mössbauer He/N_2 cryostat within an accuracy of ±0.3 K. Isomer shifts were determined relative to α-iron at 298 K.

The EPR spectrum of **4a** was recorded on a JEOL JES-FA200 continuous wave spectrometer equipped with an X-band Gunn oscillator bridge, a cylindrical mode cavity, and a nitrogen cryostat. **4a** was freshly dissolved in THF in an approximately 0.5 mM concentration in an airtight J. Young quartz EPR tube under an atmosphere of purified argon. The solution in the tube was frozen in liquid nitrogen upon exiting the glovebox and kept frozen until measured. The spectrum was measured with the following parameters: temperature 91 K, frequency 8.947895 GHz, modulation amplitude 2 mT, microwave power 0.998 mW, modulation frequency 100 kHz, time constant 0.3 s.

The EPR spectrum of **4d** was recorded on a Bruker EMX spectrometer equipped with an X-band ER 041 XG microwave bridge. **4d** was freshly dissolved in THF in an approximately 0.5 mM concentration in an airtight J. Young quartz EPR tube under an atmosphere of purified argon. The spectrum was measured with the following parameters: temperature 298 K, frequency 9.499369 GHz, modulation amplitude 0.1 mT, microwave power 0.97 mW, time constant 0.04 s. Solid-state magnetic susceptibility measurements were carried out with a superconducting quantum interference device (SQUID) magnetometer (Quantum Design, MPMS-5S) in the temperature range 2−300 K in fields of 0.01 and 1 T. Both field-cooled (FC) and zero-field-cooled (ZFC) data were obtained.

[$FeCl_2$(trop$_2$dad)] (1a). Toluene (8 mL) was added to a mixture of trop$_2$dad (500 mg, 1.15 mmol) and $FeCl_2$(thf)$_{1.5}$ (269 mg, 1.15 mmol). The reaction mixture turned green and was stirred at ambient temperature for 16 h. All volatiles were removed under reduced pressure to give a green solid, which was dried in vacuo for 3 h. Yield: 646 mg, 1.15 mmol, quantitative

DOI: 10.1021/acscatal.5b01416
ACS Catal. 2015, 5, 6230−6240

^{1}H NMR (300 MHz, CD_2Cl_2): δ 109.79 (br s, 2H), 5.03 (br s, 4 H), 3.46 (br s, 8H), 2.02 (br s, 4H), −3.91 (br s 4H), −35.42 (br s, 2 H) ppm. Mp: 208 °C dec. ATR IR: $\tilde{\nu}$ 3047 (w), 3021 (w), 1645 (w), 1600 (w), 1561 (w), 1494 (m), 1462 (w), 1437 (m), 1396 (m), 1339 (w), 1311 (m), 1263 (w), 1247 (w), 1186 (w), 1163 (m), 1115 (w), 1049 (m), 1030 (s), 1007 (m), 974 (m), 950 (m), 876 (w), 828 (m), 809 (m), 799 (s), 771 (m), 746 (s), 738 (s), 728 (s) cm^{-1}. μ_{eff} = 4.9 μ_B (Evans method). Anal. Calcd for $C_{32}H_{24}N_2FeCl_2$ (563.30 g/mol): C, 68.23; H, 4.29; N, 4.97. Found: C, 68.34; H, 4.65; N, 4.42.[50]

[Li(OEt$_2$)Fe(bis(Me$_3$SiCH$_2$)-trop$_2$dae)] (3). A solution of [$LiCH_2SiMe_3$] (85 mg, 0.90 mmol) in Et_2O (2 mL) was cooled to −30 °C and added dropwise to a suspension of **1a** (100 mg, 0.18 mmol) in Et_2O (1 mL) at −30 °C. The reaction mixture immediately turned dark brown and was warmed to room temperature. After 10 min, all volatiles were removed under reduced pressure. Toluene (1 mL) was added to the residue, and the solid part was separated by filtration. The filtrate was layered with hexanes (6 mL) and cooled to −30 °C. After 6 days, the microcrystalline solid part was isolated by filtration. It was redisolved in fluorobenzene (1.5 mL) and filtered. The filtrate was layered with hexanes (8 mL) to give microcrystalline **3** after 1 day, which was isolated by filtration and dried under a stream of argon. Yield: 36 mg, 48 μmol, 27%.

Mp: 214 °C dec. ATR IR: $\tilde{\nu}$ 3062 (w), 3015 (w), 2951 (m), 2895 (w), 2844 (w), 2809 (w), 1617 (w), 1594 (m), 1480 (m), 1458 (m), 1388 (m), 1335 (w), 1306 (w), 1245 (s), 1189 (m), 1155 (w), 1097 (m), 1065 (m), 1031 (m), 971 (m), 821 (s), 800 (s) cm^{-1}. No ^{1}H NMR resonances were detected for **3** in the range of −150 to +150 ppm in C_6D_6 as a solvent. μ_{eff} = 1.9(1) μ_B (Evans method). Anal. Calcd for $C_{44}H_{56}N_2OLiSi_2Fe$ (747.90 g/mol): C, 70.66; H, 7.55; N, 3.75. Found: C, 70.41; H, 7.67; N, 3.64.

Reaction of 1a with [CoCp$_2$]. [$CoCp_2$] (60 mg, 0.32 mmol) was added to a suspension of **1a** (100 mg, 0.15 mmol) in toluene (4 mL). The reaction mixture immediately turned from green to dark red-brown. After 2 h, solid components were separated by filtration. The filtrate was layered with hexanes (6 mL) to give a first crop of [Fe(trop$_2$dad)$_2$]·Tol. Cooling the mother liquor to −30 °C gave another crop after several days. Combined yield: 41 mg, 0.04 mmol, 53% (based on trop$_2$dad).

Analytical data were in agreement with those obtained for previously reported [Fe(trop$_2$dad)$_2$].[16] Unit cell parameters of single-crystal [Fe(trop$_2$dad)$_2$]·Tol only slightly deviate from those of [Fe(trop$_2$dad)$_2$]·1.5$THF_{1.5}$·0.5(hexanes): orthorhombic *P*; *a* = 27.0868(5) Å; *b* = 17.9322(3) Å; *c* = 21.7816(5) Å; $\alpha = \beta = \gamma = 90°$.

[Fe(trop$_2$dad)(thf)]·0.5[NaPF$_6$(THF)$_5$] (4a). $FcPF_6$ (51 mg, 154 μmol) was added to a solution of **2**·0.5(hexanes) (120 mg, 155 μmol) in THF (2 mL). After 4 h the reaction mixture was filtered and the filtrate was layered with hexanes (6 mL). After 1 day, the reaction mixture was again filtered and the filtrate was stored at −30 °C overnight to give dark red blocks of **4a** along with colorless needles. Upon warming to ambient temperature, the colorless needles dissolved and **4a** was isolated by filtration and dried under a stream of argon. Yield: 104 mg, 125 μmol, 81%.

^{1}H NMR (500 MHz, −40 °C, THF-d_8): δ 1.78 (br s, 14H, β-THF), 3.63 (br s, 14H, α-THF), 4.87 (br s, 4H, 10,11-H^{Olefin}), 5.50 (br s, 2H, 5-H^{Benzyl}), 6.95 (br s, 8H, H^{Arom}), 6.96 (br s, 4H, H^{Arom}), 6.97 (br s, 4H, H^{Arom}), 8.35 (br s, 2H, NCH) ppm. ^{13}C NMR (126 MHz, − 40 °C, THF-d_8): δ 26.20 (s, β-THF), 68.04 (s, α-THF), 78.03 (s, 5-C^{Benzyl}), 81.61 (br s, 10,11-C^{Olefin}), 123.58 (s, C^{Arom}), 126.01 (s, C^{Arom}), 126.87 (s, C^{Arom}), 127.10 (s, C^{Arom}), 138.28 (s, C^{quart}), 144.46 (s, C^{quart}), 148.94 (s, NCH) ppm. ^{1}H NMR (300 MHz, 25 °C, Tol-d_8): δ = −11.27 (br s, 2H, 5-H^{Benzyl}), − 1.01 (br s, 4H, 2,8/3,7-H^{Arom}), 1.40 (m, 14H, β-THF), 2.65 (br s, 4H, 1,9/4,6-H^{Arom}), 3.55 (m, 14H, α-THF), 6.90 (br s, 4H, 3,7/2,8-H^{Arom}), 7.76 (br s, 4H, 4,6/1,9-H^{Arom}), 55.72 (br s, 4H, 10,11-H^{Olefin}) ppm. A resonance for the HCN proton could not unambiguously identified at 25 °C (overlap with solvent signals possible). Chemical shifts are concentration dependent. ^{1}H NMR (300 MHz, −40 °C, Tol-d_8): δ 1.18 (m, 14H, β-THF), 3.30 (m, 14H, α-THF), −4.64 (s, 2H, 5-H^{Benzyl}), 6.14 (br s, 4H, 10,11-H^{Olefin}), 6.73 (br t, 4H, $^3J_{HH}$ = 7.4 Hz, 2,8/3,7-H^{Arom}), 6.96 (br t, 4H, $^3J_{HH}$ = 7.5 Hz, 3,7/2,8-H^{Arom}), 7.97 (br s, 2H, HCN, tentatively assigned, overlap with solvent signal and H^{Benzo} signal), 7.08 (br d, 4H, $^3J_{HH}$ = 7.4 Hz, 1,9/4,6-H^{Arom}), 7.15 (br d, 4H, $^3J_{HH}$ = 7.5 Hz, 4,6/1,9-H^{Arom}) ppm. Anal. Calcd for $C_{36}H_{32}FeN_2O{\cdot}0.5C_{20}H_{40}F_6NaO_5P$: Fe, 6.74. Found: Fe, 6.59.[49] ATR IR: $\tilde{\nu}$ 3065 (w), 3013 (w), 2973 (w), 2870 (w), 1595 (m), 1574 (w), 1484 (m), 1478 (m), 1463 (m), 1397 (m), 1357 (w), 1337 (w), 1302 (w), 1273 (w), 1248 (w), 1221 (w), 1204 (w), 1188 (w), 1159 (w), 1132 (w), 1099 (w), 1049 (s), 942 (w), 884 (s), 844 (s), 829 (s), 786 (s) 762 (w), 740 (s), 730 (s) cm^{-1}. Mp: 104 °C dec. UV/vis: λ_{max} 206, 264, 446 nm.

[Fe(trop$_2$dad)(MeCN)]·2(MeCN) (4b). $FcPF_6$ (26 mg, 79 μmol) was added to a solution of **2**·0.5(hexanes) (60 mg, 77 μmol) in MeCN/MTBE (2 mL, 1:3). The reaction mixture was filtered after 6 h and layered with hexanes (8 mL). After 14 h dark brown single crystals had formed and were filtered off. Small amounts of colorless solids (if present) can be removed manually or by washing with MeCN/hexanes. The product was dried under a stream of argon. Yield: 41 mg, 67 μmol, 87%.

^{1}H NMR (300 MHz, C_6D_6): δ 0.49 (br s, 9H, MeCN), 4.07 (br s, 4H, 10,11-H^{Olefin}), 5.22 (s, 2H, 5-H^{Benzyl}), 6.93−7.02 (m, 8H, H^{Arom}), 7.11 (d, 4H, $^3J_{HH}$ = 6.7 Hz, H^{Arom}), 7.33 (s, 2H, NCH), 7.39 (br s, 4H, H^{Arom}) ppm. ^{1}H NMR (500 MHz, −30 °C, MeCN-d_3): δ 1.96 (s, 9H, MeCN), 3.43 (br d, 2H, $^3J_{HH}$ = 9.6 Hz, 10/11-H^{Olefin}), 4.42 (br d, 2H, $^3J_{HH}$ = 9.6 Hz, 11/10-H^{Olefin}), 5.45 (s, 2H, 5-H^{Benzyl}), 6.91 (br t, 2H, $^3J_{HH}$ = 7.2 Hz, H^{Arom}), 7.03 (s, 4H, H^{Arom}), 7.09 (br t, 2H, $^3J_{HH}$ = 7.2 Hz, H^{Arom}), 7.16 (s, 2H, H^{Arom}), 7.24 (br d, 2H, $^3J_{HH}$ = 7.5 Hz, H^{Arom}), 7.28 (br d, 2H, $^3J_{HH}$ = 6.5 Hz, H^{Arom}), 7.42 (s, 2H, H^{Arom}), 7.59 (s, 2H, NCH) ppm. ^{13}C NMR (126 MHz, − 30 °C, CD_3CN): δ = 70.84 (s, 10/11-C^{Olefin}), 76.82 (s, 5-C^{Benzyl}), 81.17 (s, 11/10-C^{Olefin}), 122.28 (s, C^{Arom}), 125.72 (s, C^{Arom}), 125.77 (s, C^{Arom}), 126.17 (s, C^{Arom}), 126.43 (s, C^{Arom}), 127.02 (s, C^{Arom}), 127.74 (s, C^{Arom}), 127.87 (s, C^{Arom}), 144.93 (s, NCH) ppm. Quaternary carbon atoms were not detected in 1D or 2D NMR experiments, which was ascribed to poor solubility of **4b** at low temperatures. Anal. Calcd for $C_{38}H_{33}FeN_5$: Fe, 9.07. Found, Fe, 8.62.[49,50] μ_{eff} (THF-d_8, 298 K, 0.02 M) = 2.0(1) μ_B (Evans method).[51] ATR IR: $\tilde{\nu}$ 3063 (w), 3037 (w), 2919 (w), 2887 (w), 2289 (w), 2251 (m), 1593 (m), 1484 (m), 1465 (s), 1406 (m), 1371 (w), 1339 (w), 1299 (m), 1271 (w), 1243 (m), 1207 (m), 1159 (w), 1127 (w), 1100 (m), 1076 (m), 1033 (m), 978 (w), 955 (w), 890 (m), 843 (m), 825 (m), 800 (m), 770 (m), 755 (s), 744 (s), 730 (s) cm^{-1}. Mp: 136−138 °C dec. UV/vis: λ_{max} 264, 434 nm.

[Fe(trop$_2$dad)(PPh$_3$)]·(C$_6$H$_{14}$) (4c). $FcPF_6$ (26 mg, 79 μmol) and PPh_3 (41 mg, 156 μmol) were added to a solution of **2**·0.5(hexanes) (60 mg, 77 μmol) in THF (1.5 mL). After 3 h the reaction mixture was filtered and layered with hexanes

DOI: 10.1021/acscatal.5b01416
ACS Catal. 2015, 5, 6230−6240

(3.5 mL). After an additional 14 h dark brown single crystals had formed and were filtered off and dried in vacuo. Yield: 58 mg, 69 μmol, 90%.

^{1}H NMR (500 MHz, MeCN-d_3): δ 3.98 (br s, 4H, 10,11-H^{Olefin}), 5.42 (s, 2H, 5-H^{Benzyl}), 6.98 (t, 4H, $^3J_{HH}$ = 7.5 Hz, 2,8/3,7-H^{Arom}), 7.07 (t, 4H, $^3J_{HH}$ = 7.5 Hz, 3,7/2,8-H^{Arom}), 7.22 (d, 4H, $^3J_{HH}$ = 7.5 Hz, 1,9/4,6-H^{Arom}), 7.29 (br d, 6H, $^3J_{HH}$ = 7.4 Hz, *o*-Ph), 7.36−7.41 (m, 13H, 4,6/1,9-H^{Arom}, *m*-Ph, *p*-Ph), 7.63 (br s, 2H, NCH) ppm. ^{1}H NMR (500 MHz, 70 °C, MeCN-d_3): δ 4.02 (s, 4H, 10,11-H^{Olefin}), 5.41 (s, 2H, 5-H^{Benzyl}), 6.99 (t, 4H, $^3J_{HH}$ = 7.3 Hz, 2,8-H^{Arom}), 7.09 (t, 4H, $^3J_{HH}$ = 7.4 Hz, 3,7-H^{Arom}), 7.23 (d, 4H, $^3J_{HH}$ = 7.3 Hz, 1,9-H^{Arom}), 7.33−7.35 (m, 6H, $^3J_{HH}$ = 7.4 Hz, *o*/*m*-Ph), 7.38−7.40 (m, 13H, 4,6-H^{Arom}, *m*/*o*-Ph, *p*-Ph), 7.66 (br s, 2H, NCH) ppm. ^{1}H NMR (500 MHz, −30 °C, MeCN-d_3): δ 3.42 (d, 2H, $^3J_{HH}$ = 9.5 Hz, 10-H^{Olefin}), 4.41 (d, 2H, $^3J_{HH}$ = 9.5 Hz, 11-H^{Olefin}), 5.44 (s, 2H, 5-H^{Benzyl}), 6.91 (t, 2H, $^3J_{HH}$ = 7.4 Hz, 8-H^{Arom}), 7.02−7.04 (m, 4H, 2,7-H^{Arom}), 7.09 (t, 2H, $^3J_{HH}$ = 7.5 Hz, 3-H^{Arom}), 7.14−7.16 (br m, 2H, 4-H^{Arom}), 7.22−7.24 (br m, 6H, *o*-Ph), 7.24−7.27 (m, 4H, 6,9-H^{Arom}), 7.30−7.33 (m, 3H, *p*-Ph), 7.39−7.42 (m, 8H, 1-H^{Arom}, *m*-Ph), 7.56 (s, 2H, NCH) ppm. ^{13}C NMR (126 MHz, −30 °C, MeCN-d_3): δ 70.81 (s, 10-C^{Olefin}), 76.84 (s, 5-C^{Benzyl}), 81.19 (s, 11-C^{Olefin}), 122.25 (s, 8-C^{Arom}), 125.72 (s, 4-C^{Arom}), 125.77 (s, 2/7-C^{Arom}), 126.16 (s, 3-C^{Arom}), 126.45 (s, 1-C^{Arom}), 127.02 (s, 7/2-C^{Arom}), 127.73 (s, 6/9-C^{Arom}), 127.86 (s, 9/6-C^{Arom}), 129.44 (s, *m*-Ph), 129.99 (s, *p*-Ph), 135.17 (br s, *o*-Ph), 135.85 (s, 4a-C^{Arom}), 138.60 (s, *ipso*-Ph), 143.09 (s, 9a-C^{Arom}), 143.99 (s, 11a-C^{Arom}), 144.15 (s, 5a-C^{Arom}), 144.94 (s, NCH) ppm. ^{13}C NMR (126 MHz, 70 °C, MeCN-d_3): δ 77.39 (s, 10,11-C^{Olefin}), 78.61 (s, 5-C^{Benzyl}), 124.56 (s, 2,8-C^{Arom}), 126.72 (s, 1,9-C^{Arom}), 127.68 (s, 4,6-C^{Arom}), 127.97 (s, 3,7-C^{Arom}), 129.90 (s, *o*/*m*-Ph), 130.20 (s, *p*-Ph), 135.05 (s, *m*/*o*-Ph), 139.01 (s, *ipso*-Ph), 140.50 (s, 9a,11a-C^{Arom}), 145.05 (s, 4a,5a-C^{Arom}), 145.56 (s, NCH) ppm. ^{31}P NMR (203 MHz, MeCN-d_3): δ −7.36 (br s, PPh_3) ppm. Resonances for hexanes were also detected. Anal. Calcd for $C_{56}H_{53}FeN_2P$: Fe, 6.64. Found: Fe, 6.57.[49] μ_{eff}(THF-d_8, 298 K, 0.02 M) = 1.6(1) μ_B (Evans method).[51] ATR IR: $\tilde{\nu}$ 3055 (w), 3000 (w), 2953 (w), 2889 (w), 2854 (w), 1596 (m), 1574 (w), 1476 (s), 1455 (m), 1432 (s), 1377 (w), 1343 (w), 1269 (w), 1237 (w), 1188 (w), 1154 (w), 1104 (w), 1084 (m), 1066 (s), 1000 (m), 972 (w), 896 (m), 878 (m), 855 (s), 836 (s) cm^{-1}. Mp: 174 °C dec. UV/vis: λ_{max} 269, 445 nm.

[Fe(trop$_2$dad)(P(OMe)$_3$)] (4d). $FcPF_6$ (26 mg, 79 μmol) and $P(OMe)_3$ (19 mg, 153 μmol) were consecutively added to a solution of **2**·0.5(hexanes) (60 mg, 77 μmol) in THF (1 mL). After 1 h the reaction mixture was filtered and layered with hexanes (4 mL). After an additional 14 h, the reaction mixture was cooled to −30 °C. After 1 day dark brown single crystals had formed and were filtered off and dried under a stream of argon. Yield: 33 mg, 54 μmol, 70%.

^{1}H NMR (400 MHz, THF-d_8): δ 2.68 (d, 2H, $^3J_{HH}$ = 9.7 Hz, $^3J_{HP}$ = 12.6 Hz, 11-H^{Olefin}), 2.92 (d, 9H, $^3J_{HP}$ = 10.0 Hz, OMe), 3.63 (d, 2H, $^3J_{HH}$ = 9.7 Hz, $^3J_{HP}$ = 2.9 Hz, 10-H^{Olefin}), 5.42 (s, 2H, 5-H^{Benzyl}), 6.86 (t, 2H, $^3J_{HH}$ = 7.3 Hz, 3-H^{Arom}), 6.92 (t, 2H, $^3J_{HH}$ = 7.3 Hz, 8-H^{Arom}), 6.93 (t, 2H, $^3J_{HH}$ = 7.4 Hz, 7-H^{Arom}), 7.04 (t, 2H, $^3J_{HH}$ = 7.4 Hz, 2-H^{Arom}), 7.05 (d, 2H, $^3J_{HH}$ = 7.2 Hz, 4-H^{Arom}), 7.19 (d, 2H, $^3J_{HH}$ = 7.1 Hz, 6-H^{Arom}), 7.20 (s, 2H, NCH), 7.31 (d, 2H, $^3J_{HH}$ = 7.6 Hz, 1-H^{Arom}), 7.39 (d, 2H, $^3J_{HH}$ = 7.5 Hz, 9-H^{Arom}). ^{13}C NMR (100 MHz, THF-d_8): δ 52.35 (d, $^3J_{PH}$ = 8.4 Hz, $P(OMe)_3$), 61.33 (d, $^1J_{HP}$ = 12.5 Hz, 11-C^{Olefin}), 78.50 (s, 5-C^{Benzyl}), 79.27 (s, $^1J_{HP}$ = 7.2 Hz, 10-C^{Olefin}), 123.23 (s, 8-C^{Arom}), 124.49 (s, 4-C^{Arom}), 125.03 (s, 3-C^{Arom}), 125.74 (s, 6-C^{Arom}), 126.49 (s, 7-C^{Arom}), 126.61 (s, 2-C^{Arom}), 127.08 (s, 9-C^{Arom}), 128.81 (s, 1-C^{Arom}), 140.06 (d, $^3J_{HP}$ = 1.9 Hz, 4a-C^{Arom,quart}), 141.88 (s, NCH), 143.22 (s, 5a-C^{Arom,quart}), 143.28 (d, $^2J_{HP}$ = 4.4 Hz, 11a-C^{Arom,quart}), 143.41 (d, $^2J_{HP}$ = 2.7 Hz, 9a-C^{Arom,quart}) ppm. ^{31}P NMR (162 MHz, THF-d_8): δ 164.13 (br s, $P(OMe)_3$) ppm. ^{31}P{^{1}H} NMR (162 MHz, THF-d_8): δ 164.13 (br s, $P(OMe)_3$) ppm. Anal. Calcd for $C_{35}H_{33}FeN_2O_3P$: Fe, 9.06. Found: Fe, 8.61.[49,50] μ_{eff}(THF-d_8, 298 K, 0.02 M) = 0 μ_B (Evans method). **4d** is EPR silent. ATR IR: $\tilde{\nu}$ 3065 (w), 3008 (w), 2969 (w), 2936 (w), 2882 (w), 2830 (w), 1597 (m), 1574 (w), 1481 (m), 1471 (m), 1458 (m), 1441 (m), 1407 (w), 1380 (w), 1362 (w), 1346 (w), 1313 (w), 1296 (w), 1284 (w), 1270 (w), 1239 (w), 1212 (w), 1188 (m), 1103 (w), 1077 (w), 1052 (s), 1018 (s), 941 (m), 895 (m), 835 (s), 761 (s), 749 (s), 739 (s), 717 (s) cm^{-1}. Mp: >220 °C. UV/vis: λ_{max} 267, 385, 543 nm.

Reaction of 4a with Reducing Agents. The reducing agent (method A, $NaBH_4$ 6 mg, 0.16 mmol; method B, NaO*t*Bu 8 mg, 83 μmol) was added to a solution of **4a** (69 mg, 83 μmol) in THF (2 mL). After 4 h, the reaction mixture was filtered and layered with hexanes (6 mL). After 1 day, single-crystals of **2**·0.5(hexanes) were isolated by filtration and dried under a stream of argon. Cooling the filtrate to −30 °C gave a second crop of **2**. Combined yield: method A, 43 mg, 55 μmol, 66%; method B, 39 mg, 50 μmol, 60%.

Analytical data were identical with those previously reported.[16]

Catalysis. Typical experiments were carried out on the 0.24 (DMAB) and 0.31 (MAB) mmol scale (with respect to monomer). The requested amount of **2**, **4a**,**b**, or **5** was dissolved in the required solvent (3.0 mL). A solution of the monomer in the required solvent (2.0 mL for DMAB, 4.0 mL for MAB) was added through a rubber septum. For AB, typical experiments were carried out on the 0.32 mmol scale (with respect to monomer). The required amount of **2**, **4a**,**b**, or **5** was dissolved in the required solvent (3.0 mL) and added to a solution (in the case of THF) or suspension (other solvents) of the monomer in the required solvent (4.0 mL) through a rubber septum. In all cases, the gas evolved was collected in a buret setup and its volume determined. In poisoning experiments a stock solution of the poison was added at the indicated reaction time. The total volume was corrected for the volume added in this process.

DMAB. After completion of the reaction, an aliquot of the reaction mixture was analyzed by ^{11}B NMR spectroscopy after addition of 1/3 (v/v) of C_6D_6. The main component (>98%) was $(Me_2NBH_2)_2$ (catalyst **2**). ^{11}B NMR (96 MHz, Tol/C_6D_6 (2/1)): δ 4.8 (t, $^1J_{BH}$ = 113.0 Hz) ppm.

For experiments with catalyst **4a**, ^{11}B NMR analysis was carried out by performing the reaction in an NMR tube (closed system); in this case, the linear compound Me_2HN-BH_2-Me_2N-BH_3 and cyclic $(Me_2NBH_2)_2$ were detected. ^{11}B NMR (96 MHz, C_6D_6): δ −13.6 (q, $^1J_{BH}$ = 92.4 Hz, Me_2HN-BH_2-Me_2N-*B*H_3), 1.5 (t, $^1J_{BH}$ = 109.1 Hz, Me_2HN-*B*H_2-Me_2N-BH_3), 4.8 (t, $^1J_{BH}$ = 112.8 Hz, $(Me_2NBH_2)_2$) ppm.

Poly-MAB. After gas evolution had ceased, hexanes (6 mL) was added to the reaction mixture. The solid was isolated by filtration and dried in vacuo. Once isolated, the poly-MAB samples were poorly soluble in common organic solvents such as DMF, THF, toluene, and chloroform.

ATR IR: $\tilde{\nu}$ 3268 (w), 2961 (w), 2381 (m), 1618 (w), 1448 (m), 1413 (w), 1344 (s) cm^{-1}.

DOI: 10.1021/acscatal.5b01416
ACS Catal. 2015, 5, 6230−6240

Data from the reaction with 5 mol % **4a** are as follows. MALDI-TOF-MS (DCTB matrix): m/z 355.51 $[(CH_6BN)_8BH_2]^+$; 387.55 $[(CH_6BN)_9H]^+$; 398.57 $[(CH_6BN)_9BH_2]^+$; 429.61 $[(CH_6BN)_{10}H]^+$; 441.62 $[(CH_6BN)_{10}BH_2]^+$; 484.68 $[(CH_6BN)_{11}BH_2]^+$; 515.73 $[(CH_6BN)_{12}H]^+$; 527.74 $[(CH_6BN)_{12}BH_2]^+$; 569.81 $[(CH_6BN)_{13}BH_2]^+$; 601.85 $[(CH_6BN)_{14}H]^+$; 613.86 $[(CH_6BN)_{14}BH_2]^+$; 655.92 $[(CH_6BN)_{15}BH_2]^+$; 698.98 $[(CH_6BN)_{16}BH_2]^+$; 742.03 $[(CH_6BN)_{17}BH_2]^+$; 773.08 $[(CH_6BN)_{18}H]^+$; 785.09 $[(CH_6BN)_{18}BH_2]^+$; 827.15 $[(CH_6BN)_{19}BH_2]^+$; 870.21 $[(CH_6BN)_{20}BH_2]^+$; 913.27 $[(CH_6BN)_{21}BH_2]^+$; 943.31 $[(CH_6BN)_{22}H]^+$; 955.32 $[(CH_6BN)_{22}BH_2]^+$.[52]

After a reaction in toluene using 5 mol % of **4a** as a catalyst was finished, an aliquot was removed and analyzed by ^{11}B NMR spectroscopy after addition of 1/3 (v/v) of C_6D_6, revealing poly-MAB (^{11}B NMR (96 MHz, C_6D_6): δ −4.78 (unresolved t, BH_2) ppm) as the main component next to traces (<1%) of *N*-trimethylborazine (^{11}B NMR (96 MHz, C_6D_6): δ 33.8 (d, $^1J_{BH}$ = 131.5 Hz, BH) ppm).

For differentiating between chain growth and step growth mechanisms, reactions were stopped at 30% and 60% conversion, respectively. After addition of hexanes and removal of all volatiles under reduced pressure, an oily residue was obtained, which was analyzed by mass spectrometry.

Data for 30% conversion are as follows. MALDI-TOF-MS (DHB matrix): m/z 318 $[(CH_6BN)_7NH_4]^+$; 318 $[(CH_6BN)_7NH_4]^+$; 362 $[(CH_6BN)_8NH_4]^+$; 405 $[(CH_6BN)_9NH_4]^+$; 447 $[(CH_6BN)_{10}NH_4]^+$.

Data for 60% conversion are as follows. MALDI-TOF-MS (DHB matrix, m/z): 318 $[(CH_6BN)_7NH_4]^+$; 362 $[(CH_6BN)_8NH_4]^+$; 405 $[(CH_6BN)_9NH_4]^+$; 447 $[(CH_6BN)_{10}NH_4]^+$; 534 $[(CH_6BN)_{12}NH_4]^+$; 576 $[(CH_6BN)_{13}NH_4]^+$; 631 $[(CH_6BN)_{14}NH_4 - (H_2)]^+$.

Poly-AB. After gas evolution had ceased, hexanes (6 mL) was added to the reaction mixture. The solid was isolated by filtration and dried in vacuo. Once isolated, the poly-AB samples were poorly soluble in common organic solvents such as DMF, THF, toluene, and chloroform.

ATR IR: $\tilde{\nu}$ 3297 (w), 3247 (w), 2963 (w), 2362 (m), 1560 (s), 1397 (s) cm^{-1}.

After a reaction in THF using 5 mol % **4a** as a catalyst was finished, an aliquot was removed and analyzed by ^{11}B NMR spectroscopy after addition of 1/3 (v/v) of THF-d_8. Only a broad signal at ca. −2.5 ppm was detected (traces of solubilized poly-AB and/or resonance from boron species in the glass of the NMR tube). This excludes the presence of μ-aminodiborane and THF-soluble oligomers such as borazine, cyclic linear trimers, and cyclic trimers in quantities detectable in this experiment.[38a,41a,53]

Computational Methods. Geometry optimizations were carried out with the Turbomole program package[54] coupled to the PQS Baker optimizer[55] via the BOpt package,[56] at the DFT-D3/b3-lyp[57] level, employing Grimme's D3 dispersion corrections (disp3).[58] We used the def2-TZVP basis set[59] for all geometry optimizations. All minima (no imaginary frequencies) were characterized by calculating the Hessian matrix. ZPE and gas-phase thermal corrections (entropy and enthalpy, 298 K, 1 bar) from these analyses were calculated.

The geometries for the open-shell singlet (singlet biradical) minima were evaluated employing the broken-symmetry protocol. The "real" energy $\boldsymbol{\varepsilon}_s$ of the (multideterminant) open-shell singlet species was estimated from the ε_0 energies of the optimized single-determinant broken symmetry solutions and the ε_1 energies from a separate unrestricted triplet (m_s = 1) calculations at the same geometry with the same functional and basis set, using the approximate spin correction formula proposed by Noodleman and Yamagushi:[60]

$$\varepsilon_s \approx \frac{S_1^2\varepsilon_0 - S_0^2\varepsilon_1}{S_1^2 - S_0^2}$$

The optimized geometries of all species are supplied as separate files in the Supporting Information.

■ ASSOCIATED CONTENT

Supporting Information

The Supporting Information is available free of charge on the ACS Publications website at DOI: 10.1021/acscatal.5b01416.

Single-crystal X-ray analyses, Mössbauer spectroscopy, DFT calculations, isotropic shift analysis, and catalysis (PDF)
Crystallographic data for **1a** (CIF)
Crystallographic data for **3** (CIF)
Crystallographic data for **4a** (CIF)
Crystallographic data for **4b** (CIF)
Crystallographic data for **4c** (CIF)
Crystallographic data for **4d** (CIF)

■ AUTHOR INFORMATION

Corresponding Authors

*E-mail for C.L.: lichtenberg@inorg.chem.ethz.ch.
*E-mail for H.G.: hgruetzmacher@ethz.ch.

Notes

The authors declare no competing financial interest.

■ ACKNOWLEDGMENTS

The authors thank M. Sc. J. Bloch for experimental contributions and Dr. L. Viciu for SQUID analyses. A Feodor-Lynen Fellowship to C. L. generously hosted by Prof. Dr. François Diederich is gratefully acknowledged. Financial support by the Swiss National Science Foundation (SNF) and the ETH is gratefully acknowledged.

■ REFERENCES

(1) (a) Gray, H. B.; Williams, R.; Bernal, I.; Billig, E. *J. Am. Chem. Soc.* **1962**, *84*, 3596−3597. (b) Gray, H. B.; Billig, E. *J. Am. Chem. Soc.* **1963**, *85*, 2019−2020. (c) Davison, A.; Edelstein, N.; Holm, R. H.; Maki, A. H. *J. Am. Chem. Soc.* **1963**, *85*, 2029−2030.

(2) (a) Lyaskovskyy, V.; de Bruin, B. *ACS Catal.* **2012**, *2*, 270−279. (b) Luca, O. R.; Crabtree, R. H. *Chem. Soc. Rev.* **2013**, *42*, 1440−1459.

(3) Chirik, P. J.; Wieghardt, K. *Science* **2010**, *327*, 794−795.

(4) Leibfritz, D.; tom Dieck, H. *J. Organomet. Chem.* **1976**, *105*, 255−261.

(5) tom Dieck, H.; Bruder, H. *J. Chem. Soc., Chem. Commun.* **1977**, 24−25.

(6) (a) Muresan, N.; Lu, C. C.; Gosh, M.; Peters, J. C.; Abe, M.; Henling, L. M.; Weyhermüller, T.; Bill, E.; Wieghardt, K. *Inorg. Chem.* **2008**, *47*, 4579−4590. (b) Khusniyarov, M. M.; Weyhermüller, T.; Bill, E.; Wieghardt, K. *J. Am. Chem. Soc.* **2009**, *131*, 1208−1221.

(7) Substitution of one or both dad ligands for the related doubly deprotonated *o*-phenylenediamine ligands leads to different electronic structures of the resulting complexes.[6b]

(8) Bart, S. C.; Hawrelak, E. J.; Lobkovsky, E.; Chirik, P. J. *Organometallics* **2005**, *24*, 5518−5527.

(9) (a) tom Dieck, H.; Dietrich, J. *Angew. Chem.* **1985**, *97*, 795−796; *Angew. Chem., Int. Ed. Engl.* **1985**, *24*, 781−783. (b) Le Floch, P.;

DOI: 10.1021/acscatal.5b01416
ACS Catal. 2015, 5, 6230−6240

Knoch, F.; Kremer, F.; Mathey, F.; Scholz, J.; Scholz, W.; Thiele, K.-H.; Zenneck, U. *Eur. J. Inorg. Chem.* **1998**, *1998*, 119−126.
(10) tom Dieck, H.; Diercks, R. *Angew. Chem.* **1983**, *95*, 801−802; *Angew. Chem., Int. Ed. Engl.* **1983**, *22*, 778−779.
(11) O'Reilly, R. K.; Shaver, M. P.; Gibson, V. C.; White, A. J. P. *Macromolecules* **2007**, *40*, 7441−7452.
(12) Rodríguez-Lugo, R. E.; Trincado, M.; Vogt, M.; Tewes, F.; Santiso-Quinones, G.; Grützmacher, H. *Nat. Chem.* **2013**, *5*, 342−347.
(13) (a) Lichtenberg, C.; Viciu, L.; Adelhardt, M.; Sutter, J.; Meyer, K.; de Bruin, B.; Grützmacher, H. *Angew. Chem.* **2015**, *127*, 5858−5863; *Angew. Chem., Int. Ed.* **2015**, *54*, 5766−5771. (b) Lichtenberg, C.; Adelhardt, M.; Wörle, M.; Büttner, T.; Meyer, K.; Grützmacher, H. *Organometallics* **2015**, *34*, 3079−3089.
(14) Vance, J. R.; Schäfer, A.; Robertson, A. P. M.; Lee, K.; Turner, J.; Whittell, G. R.; Manners, I. *J. Am. Chem. Soc.* **2014**, *136*, 3048−3064.
(15) Depending on the Fe precursor and the reaction conditions, the in situ formed Fe particles can also be catalytically active (cf. ref 14).
(16) Lichtenberg, C.; Viciu, L.; Vogt, M.; Rodríguez-Lugo, R. E.; Adelhardt, M.; Sutter, J.; Khusniyarov, M. M.; Meyer, K.; de Bruin, B.; Bill, E.; Grützmacher, H. *Chem. Commun.* **2015**, *51*, 13890.
(17) Bart, S. C.; Hawrelak, E. J.; Schmisseur, A. K.; Lobkovsky, E.; Chirik, P. J. *Organometallics* **2004**, *23*, 237−246.
(18) τ_5 values ranging from 0 to 1 are possible, where 0 and 1 indicate perfect square-pyramidal and trigonal-bipyramidal coordination geometries, respectively: Addison, A. W.; Rao, T. N.; Reedijk, J.; van Rijn, J.; Verschoor, G. C. *J. Chem. Soc., Dalton Trans.* **1984**, 1349−1356.
(19) (a) de Lange, P. P. M.; Kraakman, M. J. A.; van Wijnkoop, M.; Frühauf, H.-W.; Vrieze, K. *Inorg. Chim. Acta* **1992**, *196*, 151−160. (b) Frühauf, H.-W.; Wolmershäuser, G. *Chem. Ber.* **1982**, *115*, 1070−1082. (c) Kokkes, M. W.; Stufkens, D. J.; Oskam, A. *J. Chem. Soc., Dalton Trans.* **1983**, 439−445.
(20) It should be noted, however, that for compounds with pyridine-based potentially redox active ligands it has been shown that ligand structural parameters might not always be sufficient for an oxidation state assignment of the metal center: see ref 25b.
(21) Gütlich, P.; Bill, E.; Trautwein, A. X. *Mössbauer Spectroscopy and Transition Metal Chemistry*; Springer: Heidelberg, Germany, 2011.
(22) Chłopek, K.; Bill, E.; Weyhermüller, T.; Wieghardt, K. *Inorg. Chem.* **2005**, *44*, 7087−7098.
(23) Attempts to isolate **4e**, e.g. by exposing **4a**,**b** (neat substances or toluene solutions) to reduced pressure, have so far been unsuccessful.
(24) Budzelaar, P. H. M.; de Bruin, B.; Gal, A. W.; Wieghardt, K. E.; van Lenthe, J. H. *Inorg. Chem.* **2001**, *40*, 4649−4655.
(25) (a) Zell, T.; Milko, P.; Fillman, K. L.; Diskin-Posner, Y.; Bendikov, T.; Iron, M. A.; Leitus, G.; Ben-David, Y.; Neidig, M. L.; Milstein, D. *Chem. - Eur. J.* **2014**, *20*, 4403−4413. (b) Butschke, B.; Fillman, K. L.; Bendikov, T.; Shimon, L. J. W.; Diskin-Posner, Y.; Leitus, G.; Gorelsky, S. I.; Neidig, M. L.; Milstein, D. *Inorg. Chem.* **2015**, *54*, 4909−4926.
(26) Samples of **4a** from one and the same batch are diamagnetic in the solid state (SQUID) but show an effective magnetic moment >0 in solution (Evans method).
(27) Compounds $\mathbf{4e}^{\mathbf{OSS}}$ and $\mathbf{4e}^{\mathbf{triplet}}$ are close in energy according to DFT calculations (see Table 3). Single-point calculations with COSMO dielectric corrections and a solution-phase reference volume (1 mol in 1 L) gave a free energy of +6.3 kcal/mol for the reaction $\mathbf{4a}^{\mathbf{OSS}} \rightarrow \mathbf{4e}^{\mathbf{triplet}}$ + THF. This can be taken as an additional hint toward the suggested equilibrium scenario.
(28) In agreement with these observations, **4a** shows paramagnetically shifted ^{1}H NMR resonances in nondonor solvents which are shifted toward the "diamagnetic chemical shift range" upon switching to donor solvents, using higher concentrations of **4a**, or cooling the sample.
(29) Due to the small differences in the effective magnetic moments of **4a**−**c** in solution, the errors associated with the Evans method, and the possibility of trace impurities influencing the effective magnetic moment, we refrain from drawing conclusions concerning the equilibrium constants of singlet/triplet equilibria for **4a**−**c** merely on the basis of data obtained using the Evans method.
(30) Scheidt, W. R.; Reed, C. A. *Chem. Rev.* **1981**, *81*, 543−555.
(31) Eames, E. V.; Harris, T. D.; Betley, T. A. *Chem. Sci.* **2012**, *3*, 407−415.
(32) Recently, a coordination-induced spin state change has also been reported for a Mn^{5+} nitride complex: Kropp, H.; Scheurer, A.; Heinemann, F. W.; Bendix, J.; Meyer, K. *Inorg. Chem.* **2015**, *54*, 3562−3572.
(33) E.g.: (a) Keaton, R. J.; Blacquiere, J. M.; Baker, R. T. *J. Am. Chem. Soc.* **2007**, *129*, 1844−1845. (b) Staubitz, A.; Presa Soto, A.; Manners, I. *Angew. Chem.* **2008**, *120*, 6308−6311; *Angew. Chem., Int. Ed.* **2008**, *47*, 6212−6215.
(34) (a) Stephens, F. H.; Pons, V.; Baker, R. T. *Dalton Trans.* **2007**, 2613−2626. (b) Staubitz, A.; Robertson, A. P. M.; Manners, I. *Chem. Rev.* **2010**, *110*, 4079−4124. (c) Clark, T. J.; Lee, K.; Manners, I. *Chem. - Eur. J.* **2006**, *12*, 8634−8648. (d) Alcaraz, G.; Sabo-Etienne, S. *Angew. Chem.* **2010**, *122*, 7326−7335; *Angew. Chem., Int. Ed.* **2010**, *49*, 7170−7179.
(35) Jaska, C. A.; Manners, I. *J. Am. Chem. Soc.* **2004**, *126*, 2698−2699.
(36) Johnson, H. C.; Leitao, E. M.; Whittell, G. R.; Manners, I.; Lloyd-Jones, G. C.; Weller, A. S. *J. Am. Chem. Soc.* **2014**, *136*, 9078−9093.
(37) Liu, Z.; Song, L.; Zhao, S.; Huang, J.; Ma, L.; Zhang, J.; Lou, J.; Ajayan, P. M. *Nano Lett.* **2011**, *11*, 2032−2037.
(38) For the catalyzed synthesis of $[MeHN\text{-}BH_2]_3$ and $[MeN\text{-}BH]_3$ see: (a) Jaska, C. A.; Temple, K.; Lough, A. J.; Manners, I. *Chem. Commun.* **2001**, 962−963. (b) Jaska, C. A.; Temple, K.; Lough, A. J.; Manners, I. *J. Am. Chem. Soc.* **2003**, *125*, 9424−9434. (c) Kawano, Y.; Uruichi, M.; Shimoi, M.; Taki, S.; Kawaguchi, T.; Kakizawa, T.; Ogino, H. *J. Am. Chem. Soc.* **2009**, *131*, 14946−14957. (d) Reference 41a..
(39) (a) Dietrich, B. L.; Goldberg, K. I.; Heinekey, D. M.; Autrey, T.; Linehan, J. C. *Inorg. Chem.* **2008**, *47*, 8583−8585. (b) Staubitz, A.; Sloan, M. E.; Robertson, A. P. M.; Friedrich, A.; Schneider, S.; Gates, P. J.; Schmedt auf der Günne, J.; Manners, I. *J. Am. Chem. Soc.* **2010**, *132*, 13332−13345. (c) Dallanegra, R.; Robertson, A. P. M.; Chaplin, A. B.; Manners, I.; Weller, A. S. *Chem. Commun.* **2011**, *47*, 3763−3765.
(40) Poly-MAB can also be obtained as follows. (a) From MAB with stoichiometric amounts of skeletal Ni: Robertson, A. P. M.; Suter, R.; Chabanne, L.; Whittell, G. R.; Manners, I. *Inorg. Chem.* **2011**, *50*, 12680−12691. (b) From $[MeH_2NBH_2(OEt_2)][B(C_6F_5)_4]$ and 10 equiv of 2,6-di-*tert*-butylpyridine: Metters, O. J.; Chapman, A. M.; Robertson, A. P. M.; Woodall, C. H.; Gates, P. J.; Wass, D. F.; Manners, I. *Chem. Commun.* **2014**, *50*, 12146−12149.
(41) (a) Vance, J. R.; Robertson, A. P. M.; Lee, K.; Manners, I. *Chem. - Eur. J.* **2011**, *17*, 4099−4103. (b) Kakizawa, T.; Kawano, Y.; Naganeyama, K.; Shimoi, M. *Chem. Lett.* **2011**, *40*, 171−173.
(42) A turnover frequency of 3.66 s^{-1} was determined for the dehydrogenation of AB, heterogeneously catalyzed by in situ generated Fe particles.[48a]
(43) When 20 equiv of MAB was reacted with **4a** on NMR scale in C_6D_6, the ^{1}H NMR spectrum recorded after full conversion showed paramagnetically shifted resonances, which were not identical with those of **4a**. This is in agreement with **4a** acting as a precatalyst. After addition of another 20 equiv of MAB, the relative intensity of the paramagnetically shifted ^{1}H NMR resonances had changed, suggesting that (partial) catalyst degradation takes place. Similarly, new paramagnetically shifted resonances were observed, the relative intensity of which changed in the course of the reaction, when DMAB was used as a substrate.
(44) Another possibility to explain reduced catalyst activity would be precipitation of the active species with the growing polymer. This possibility was ruled out because filtration of the reaction mixture after dehydrogenation of 20 equiv of MAB did not yield significant amounts of solids. Furthermore, the filtrate showed the same catalytic activity upon addition of another 20 equiv of MAB, as observed in the same experiment without filtration.

DOI: 10.1021/acscatal.5b01416
ACS Catal. 2015, 5, 6230−6240

(45) For studies of Fe-based catalysts operating homogeneously or heterogeneously in AB and DMAB dehydrogenation, see refs 13a, 14, and 48.
(46) Crabtree, R. H. *Chem. Rev.* **2012**, *112*, 1536−1554.
(47) Selective poisoning experiments with 0.1 equiv of $P(OMe)_3$ per Fe only marginally decreased the rate of the reaction, suggesting homogeneous reaction conditions.
(48) (a) Sonnenberg, J. F.; Morris, R. H. *ACS Catal.* **2013**, *3*, 1092−1102. (b) Baker, R. T.; Gordon, J. C.; Hamilton, C. W.; Henson, N. J.; Lin, P.-H.; Maguire, S.; Murugesu, M.; Scott, B. L.; Smythe, N. C. *J. Am. Chem. Soc.* **2012**, *134*, 5598−5609.
(49) Accurate results from combustion analysis proved to be difficult to obtain for compounds **4a**−**d**. Alternative bulk methods of characterization are provided as evidence of the efficacy of the syntheses.
(50) Minor deviations from expected values are ascribed to trace amounts of residual solvent molecules.
(51) Minor contributions to the observed μ_{eff} due to (super) paramagnetic impurities cannot strictly be excluded.
(52) Formation of a poly-MAB species with a "BH_2^+" end group could invoke B−N bond cleavage as part of the polymerization mechanism or occur during the ionization process of the mass spectrometric analysis.
(53) Gaines, D. F.; Schaeffer, R. *J. Am. Chem. Soc.* **1964**, *86*, 1505−1507.
(54) Ahlrichs, R. *Turbomole Version 6.5*, Theoretical Chemistry Group, University of Karlsruhe.
(55) *PQS version 2.4*; Parallel Quantum Solutions, Fayettevile, AR, USA, 2001. The Baker optimizer is available separately from PQS upon request: Baker, I. *J. Comput. Chem.* **1986**, *7*, 385−395.
(56) Budzelaar, P. H. M. *J. Comput. Chem.* **2007**, *28*, 2226−2236.
(57) (a) Lee, C.; Yang, W.; Parr, R. G. *Phys. Rev. B: Condens. Matter Mater. Phys.* **1988**, *37*, 785−789. (b) Becke, A. D. *J. Chem. Phys.* **1993**, *98*, 1372−1377. (c) Becke, A. D. *J. Chem. Phys.* **1993**, *98*, 5648−5652. (d) Calculations were performed using the Turbomole functional "b3-lyp", which is not completely identical with the Gaussian "B3LYP" functional..
(58) Grimme, S.; Antony, J.; Ehrlich, S.; Krieg, H. *J. Chem. Phys.* **2010**, *132*, 154104.
(59) (a) Weigend, F.; Ahlrichs, R. *Phys. Chem. Chem. Phys.* **2005**, *7*, 3297−3305. (b) Weigend, F.; Häser, M.; Patzelt, H.; Ahlrichs, R. *Chem. Phys. Lett.* **1998**, *294*, 143−152.
(60) (a) Knijnenburg, Q.; Hetterscheid, D.; Kooistra, T. M.; Budzelaar, P. H. M. *Eur. J. Inorg. Chem.* **2004**, *2004*, 1204. (b) Goldstein, E.; Beno, B.; Houk, K. N. *J. Am. Chem. Soc.* **1996**, *118*, 6036. (c) Yamanaka, S.; Kawakami, T.; Nagao, H.; Yamaguchi, Y. *Chem. Phys. Lett.* **1994**, *231*, 25.

DOI: 10.1021/acscatal.5b01416
ACS Catal. 2015, 5, 6230−6240